Heterogeneous Catalysis through Subsurface Sites

V. Ledentu, W. Dong, and P. Sautet*

Contribution from the Institut de Recherches sur la Catalyse, Centre National de la Recherche Scientifique, 2 Av. Albert Einstein, 69626 Villeurbanne, France, and Laboratoire de Chimie Théorique, École Normale Supérieure de Lyon, 46, Allée d'Italie, 69364 Lyon Cedex 07, France

Received November 17, 1998

Abstract: Experimental evidences are now accumulating and reveal that subsurface species can play an important role in heterogeneous catalysis. Recently, it has been found experimentally that, on the Ni(111) surface, CH_3 is hydrogenated selectively by subsurface hydrogen. We report here a detailed study of this prototype reaction for the heterogeneous catalysis through subsurface sites by using a theoretical approach. The elementary steps involved are identified, and a detailed analysis of the reaction pathways allows us to understand the microscopic mechanism. The results obtained here highlight the general features of the new mechanism of heterogeneous catalysis through subsurface sites.

I. Introduction

Nowadays, there are two widely accepted mechanisms of heterogeneous catalysis: Langmuir−Hinshelwood and Eley-Rideal mechanisms.[1] Through the former, all reactants are first adsorbed on a catalyst surface and then react with each other. Through the latter, only some reactants are adsorbed and chemical reactions take place between adsorbates and reactants in the gas phase. Recently, another type of mechanism of heterogeneous catalysis has been discovered. In a pioneering work,[2] Ceyer and co-workers have shown unambiguously that the hydrogenation of CH_3 on a Ni(111) surface takes place with subsurface hydrogen atoms. It was found that the subsurface hydrogen species have a catalytic activity quite different from that of the surface species. Now, other examples of catalytic reactions through subsurface sites are accumulating. In a subsequent work, Ceyer and co-workers have shown that the hydrogenation of ethylene on Ni(111) takes place also with subsurface hydrogen.[3] Catalytic reactions with subsurface species are limited to neither the hydrogenation reaction nor the Ni catalyst only. Very recently, Millar et al. have found that, on a Ag catalyst, the subsurface oxygen atoms play a key role in the oxidation of methanol into formaldehyde.[4] Another example of heterogeneous catalysis through subsurface sites is provided by Rothaemel et al.[5] for CO on Pd reacting with subsurface hydrogen to form CHO. Although it is now established experimentally that subsurface species can take an active part in a variety of heterogeneous catalytic reactions, many fundamental questions for the mechanism of such reactions are still open. Why are subsurface species sometimes more reactive than their surface counterparts? How is the reaction pathway involving subsurface species different from that with surface species only? Do the emerging of the subsurface species and the formation of products proceed in a concerted way or do they constitute two separate steps? Although some conjectures have been made on the basis of experimental observations and intuition,[2] a microscopic understanding is still lacking for the mechanism of catalysis through subsurface sites. In this paper, these issues are addressed by using a theoretical approach.

II. Theoretical Approach

The results presented in this paper are obtained by using an ab initio quantum mechanical method based on density functional theory. We perform an iterative solution of the Kohn−Sham equations of the density-functional theory using residuum-minimization methods or sequential band-by-band conjugate gradient techniques and optimized charge-density mixing routines.[6] The exchange-correlation functional used is the Perdew−Zunger parametrization[7] of the quantum Monte Carlo simulations performed by Ceperley and Alder.[8] The generalized gradient approximation (GGA) proposed by Perdew and Wang[9] is also included in the self-consistent procedure, i.e., not by adding only a GGA correction based on the LDA electron density. This theoretical approach has been applied recently to study some simple surface reactions and leads to qualitatively correct results. For example, for the dissociation of H_2 on Cu(111),[10] the local density approximation (LDA) predicts a nearly nonactivated dissociation while the activation barrier of the GGA is consistent with the estimation from molecular beam experiments.[11−14] The GGA used in our previous studies of the

* To whom correspondence should be addressed at the Centre National de la Recherche Scientifique.

(1) Somorjai, G. A. *Introduction to Surface Chemistry and Catalysis*; John Wiley & Sons Inc.: New York, 1994.

(2) Johnson, A. D.; Daley, S. P.; Utz, A. L.; Ceyer, S. T. *Science* **1994**, *257*, 223.

(3) Daley, S. P.; Utz, A. L.; Trautman, T. R.; Ceyer, S. T. *J. Am. Chem. Soc.* **1994**, *116*, 6001.

(4) Millar, G. J.; Nelson, M. L.; Uwins, P. J. R. *J. Catal.* **1997**, *169*, 143.

(5) Rothaemel, M.; Zanthoff, H. W.; Baerns, M. *Catal. Lett.* **1994**, *28*, 321.

(6) The computation method is implemented in the Vienna Ab initio Simulation Program (VASP). More details for technical aspects can be found from the following: (a) Kresse, G.; Hafner, J. *Phys. Rev. B* **1994**, *49*, 14251. (b) Kresse, G.; Furthmüller, *J. Comput. Mater. Sci.* **1996**, *6*, 15.

(7) Perdew, J. P.; Zunger, A. *Phys. Rev. B* **1981**, *43*, 5048.

(8) Ceperley, D. M.; Alder, B. *Phys. Rev. Lett.* **1980**, *45*, 566.

(9) Perdew, J. P.; Chevary, J. A.; Vosko, S. H.; Jackson, K. A.; Pederson, M. R.; Singh, D. J.; Fiolhais, C. *Phys. Rev. B* **1992**, *46*, 6671.

(10) Hammer, B.; Scheffler, M.; Jacobsen, K. W.; Nøskov, J. K. *Phys. Rev. Lett.* **1994**, *73*, 1400.

(11) Anger, G.; Winkler, A.; Rendulic K. D. *Surf. Sci.* **1989**, *220*, 1.

(12) Berger, H. F.; Leisch, M.; Winkler, A.; Rendulic K. D. *Chem. Phys. Lett.* **1990**, *175*, 425.

(13) Hayden, B. E.; Lamont, C. L. A. *Phys. Rev. Lett.* **1989**, *63*, 1823.

(14) Rettner, C. T.; Auerbach, D. J.; Michelsen, H. A. *Phys. Rev. Lett.* **1992**, *68*, 1164 and 2547.

10.1021/ja983975g CCC: $19.00
Published on Web 02/08/2000

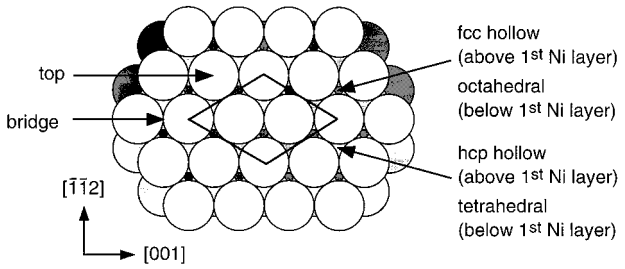

Figure 1. Top view of the Ni(111) surface with the adsorption sites and the $(\sqrt{3} \times \sqrt{3})R30°$ unit cell.

dissociation of H_2 on palladium surfaces[15,16] reveals the existence of some nonactivated dissociation pathways. This also conforms to the results of molecular beam experiments which show that H_2 has high sticking probabilities on Pd(111) and Pd(110) surfaces.[17,18] In the approach used here, the valence orbitals are expanded with plane waves. The electron−ion interaction is described by ultrasoft pseudopotentials.[19,20] In the last years, it has been shown that such pseudopotentials are very successful in both the study of a series of transition metal surfaces and the chemisorptions and in simple reactions on these surfaces.[15,16,21−23] Thanks to the efficiency of the ultrasoft pseudopotentials, the plane-wave expansion can be truncated at a cutoff energy equal to 280 eV. To model a surface, we adopt the periodic slab supercell approach. Test calculations are made to show that converged results can be obtained from a 4-layer slab. A vacuum space corresponding to 6 Ni layers, i.e., 12.2 Å, is used to separate the central slab and its periodic images. To assess the effect of the spurious dipolar interaction between the periodic images, we carried out test calculations with symmetric (adsorbates on the two surfaces of the slab) and asymmetric (adsorbates on only one surface) slabs. It is found that the spurious dipolar interaction is negligible since we obtain nearly the same results with a symmetric or an asymmetric slab. Most calculations are made with a $(\sqrt{3} \times \sqrt{3})R30°$ surface cell which contains 3 Ni atoms per layer (see Figure 1). To examine the effect of the adsorbate concentration, some calculations are performed with larger cells, i.e., (2×2) and (3×3) cells which contain respectively 4 and 9 Ni atoms per layer. No appreciable dependency on the unit cell size is found; e.g., the energy barrier for the emerging of H from a subsurface site to the surface changes from 0.18 to 0.15 eV when the coverage changes from $\theta = {}^1/_3$ ML (monolayer) corresponding to the $(\sqrt{3} \times \sqrt{3})R30°$ unit cell to $\theta = {}^1/_9$ ML corresponding to the (3×3) unit cell. Brillouin-zone integrations have been performed on a $5 \times 5 \times 1$ grid of Monkhorst−Pack points[24] for a $(\sqrt{3} \times \sqrt{3})R30°$ cell, and the grid is reduced proportionally for larger cells. Careful test calculations are carried out, and an overall convergence of 10^{-3} Rydbergs for the cohesive energy of the bulk solid, surface, and adsorption energies is reached under the computational conditions described above. The conjugate-gradient method is applied to the geometry optimization of the structures corresponding to a minima on the potential energy surface. The positions of the metal atoms in the two top layers of the slab are fully optimized. Test calculations are made to show that the optimization of deeper layers has only a very small effect on the surface reaction studied here since the forces on these layers are negligible. For transition states along different reaction paths, the nudged elastic band method[25] is first used to get a rough localization. This method consists of making a chain between the structures corresponding to the reactants and the products of the considered reaction. The optimization of a number of intermediate points on this chain is performed along the direction perpendicular to the chain. After this optimization, the highest intermediate point gives a first estimation of the transition state. Then, the transition state is refined in such a way that all the forces are made equal to zero by using a quasi-Newton method with constraints. Finally, the Hessian is calculated (via finite difference of the analytical forces) near the located stationary point and the diagonalization of the Hessian allows us to characterize the stationary point. It is to be emphasized that the transition points found in the above way are guaranteed to connect to the relevant reactant and product by the construction of the nudged elastic band method. It is worth to point out that in many surface reactions the formed product desorbes from the surface. In this case, the final product state is chosen at a sufficient large (but finite) distance from the surface so that the interaction between the product and the surface is negligible and a finite chain can be used in the nudged elastic band method. Spin polarization is taken into account for radical species such as H and CH_3. For stable and transition states of adsorbates on surface or subsurface sites, the effect of the spin polarization is negligible for bond length and does not exceed 15% of the binding energies. To reduce computational costs, most calculations are performed without spin polarization.

III. Results and Discussions

In the present work, we consider the hydrogenation of CH_3 by subsurface hydrogen on the Ni(111) surface[2] as a prototype of the catalysis through subsurface sites. Before investigating this reaction, we have characterized the different species involved, i.e., H_2, CH_4, and clean Ni(111). Then, the adsorption and coadsorption of H and CH_3 on Ni(111) are examined. Finally, a variety of reaction pathways will be studied in detail to reveal the reaction mechanism.

A. Bulk Ni, Clean Surface and Isolated Reactants. For the bulk Ni, we have calculated the cohesive energy, the lattice constant, and the elastic modulus and found respectively 5.21 eV/Ni atom, 3.523 Å, and 205 GPa. These results are in reasonably good agreement with the experimental results,[26,27] 4.43 eV/Ni atom, 3.524 Å, and 186 GPa.

Since Ni(111) is a quite compact surface, the top layer undergoes only very small inward relaxation. From the experimental work of Lu et al.,[28] it is estimated that the relaxation must be less than 2%. Our calculation gives an inward relaxation of 0.6% in good agreement with the experimental estimation. For the surface energy and the work function, we obtain respectively 0.68 eV/atom and 5.26 eV where the corresponding experimental values are 0.82 eV/atom[29] and 5.35 eV.[30]

For H_2, we have obtained a bond length of 0.747 Å, a bond energy of 4.46 eV, and a vibrational frequency of 4420 cm^{-1} which are in remarkably good agreement with the experimental values ($d_{H-H} = 0.7414$ Å, $E = 4.476$ eV, and $\nu = 4400$ cm^{-1}).[31] For methane, the C−H bond length and the first dissociation energy, i.e., $CH_4 \rightarrow CH_3 + H$, from our calculations are 1.095 Å and 4.80 eV. The experimental values are 1.094 Å[32] and

(15) Dong, W.; Hafner, J. *Phys. Rev. B* **1997**, *56*, 15396.
(16) Ledentu, V.; Dong, W.; Sautet, P. *Surf. Sci.* **1998**, *412/413*, 518.
(17) Resch, C.; Berger, H. F.; Rendulic, K. D.; Bertel, E. *Surf. Sci.* **1994**, *316*, L1105.
(18) Beutl, M.; Riedler, M.; Rendulic, K. D. *Chem. Phys. Lett.* **1995**, *247*, 249.
(19) Vanderbilt, D. *Phys. Rev. B* **1990**, *41*, 7892.
(20) Kresse, G.; Hafner, J. *J. Phys.: Condens. Matter* **1994**, *6*, 8245.
(21) Dong, W.; Kresse, G.; Furthmüller, J.; Hafner, J. *Phys. Rev. B* **1996**, *54*, 2157.
(22) Ledentu, V.; Dong, W.; Sautet, P.; Kresse, G.; Hafner, J. *Phys. Rev. B* **1998**, *57*, 12482.
(23) Dong, W.; Ledentu, V.; Sautet, P.; Eichler, A.; Hafner, J. *Surf. Sci.* **1998**, *411*, 123.
(24) Monkhorst, H. J.; Pack, J. D. *Phys. Rev. B* **1976**, *13*, 5188.
(25) Mills, G.; Jonsson, H.; Schenter, G. K. *Surf. Sci.* **1995**, *324*, 305.
(26) Kittel, K. *Introduction to Solid State Physics*, 4th ed., John Wiley and Sons: New York, 1971; pp 96, 143.
(27) Wyckoff, R. W. G. *Crystal Structures*; Interscience Publishers: New York, 1960; Vol. I.
(28) Lu, H. C.; Gusev, E. P.; Garfunkel, E. *Surf. Sci.* **1996**, *352−354*, 21.
(29) Michaelson, H. B. *J. Appl. Phys.* **1977**, *48*, 4729.
(30) Baker, B. G.; Johnson, B. B.; Maire, G. L. C. *Surf. Sci.* **1971**, *24*, 572.
(31) Huber, K. P.; Herzberg, G. *Molecular Spectra and Molecular Structure Constants of Diatomic Molecules*; Van Nostrand: New York, 1979.
(32) Gray, D. L.; Robiette, A. G.; Pine, A. S. J. *Mol. Spectrosc.* **1979**, *77*, 440.

Table 1. Energies and Geometries for the $(\sqrt{3} \times \sqrt{3})R30°$ Chemisorption of H or CH_3 on Ni(111) (Coverage $^1/_3$ ML)

adsorption site[a]	E_{ad} (eV)[b]	d_{ad-Ni} (Å)[c]	z_{ad} (Å)[d]	Δd_{12} (%)[e]
fcc hollow (H)	−0.66	1.70	0.91	−0.1
hcp hollow (H)	−0.65	1.70	0.91	−0.1
bridge (H)	−0.52	1.62	1.03	−0.1
top (H)	−0.04	1.46	1.46	−0.4
octahedral (H)	+0.05	1.83	−0.95	+3.7
fcc (CH_3, top)	−1.98	2.12	1.56	0.0
fcc (CH_3, hcp)	−1.64	2.23	1.70	−0.4
hcp (CH_3, top)	−1.95	2.13	1.57	0.0
hcp (CH_3, fcc)	−1.63	2.25	1.73	−0.4
top (CH_3, hcp)	−1.79	1.97	1.97	0.0
top (CH_3, fcc)	−1.79	1.97	1.97	−0.4

[a] The adsorbed species is put in parentheses. For CH_3, the first site label indicates the location of the C atom and the second site label in parentheses indicates the sites toward which the H atoms of the CH_3 group are oriented. [b] Adsorption energies are defined as $E_{ad}^{H} = E_{H/Ni(111)} - E_{Ni(111)} - {}^1/_2E_{H_2}$ and $E_{ad}^{CH_3} = E_{CH_3/Ni(111)} - E_{Ni(111)} - E_{CH_3}$ for the adsorption of H and CH_3, respectively. $E_{Ni(111)}$, E_{H_2} and E_{CH_3} are calculated values for the clean Ni(111) surface, H_2 molecule, and CH_3 including spin polarization. [c] d_{ad-Ni}: bond length between the adsorbates (H or CH_3) and its nearest Ni atoms on the top layer. [d] z_{ad}: height of the adsorbates (H or CH_3) with respect to the first nickel layer. [e] Δd_{12}: relative relaxation of the spacing between the two first nickel layers.

4.54 eV.[33] Again, a very good agreement is found. We recall here that our approach is designed primarily for periodic systems. The calculations for an isolated reactant are performed by putting it in a large empty box to avoid the interaction between periodic images. So, from the computational point of view, these calculations are as heavy as those for chemisorption.

B. Adsorption and Coadsorption of H and CH_3 on Ni(111). The 3-fold hollow sites are the most stable adsorption sites for both reactants. This conforms to the general tendency of chemisorption for atoms; i.e., the higher the coordination number of a site, the more stable it will be. There is a slightly stronger bonding on the fcc sites than on the hcp sites. At the coverage of $^1/_3$ ML, we have found an adsorption energy equal to −0.66 eV for H atoms on the fcc site without zero point energy corrections (see Table 1 for a definition of the adsorption energy). The experimental result is −0.50 eV.[34] For H atoms absorbed on the subsurface octahedral sites between the two top Ni layers, the adsorption energy is 0.05 eV. Since the emerging of the subsurface H atoms has an energy barrier (to be shown later), the metastable state corresponding to the adsorption on subsurface sites can be prepared experimentally.[2] The adsorption energies for both surface and subsurface situations are almost independent of the coverage with the variation being less than 30 meV for the coverages from $^1/_9$ ML to 1 ML. The most stable adsorption geometry for the methyl group is that with the C atom on a fcc site and the H atoms oriented toward the nearby top sites. All of the above results for the chemisorption of H and CH_3 are summarized in Table 1.

To characterize the possible starting configurations of the hydrogenation reaction of CH_3 by surface and subsurface H atoms, we have examined two coadsorption patterns: one with the methyl on a fcc site and the H atom on an octahedral subsurface site and the other with the H atom on a surface site (see Figure 2). First, the case of the hydrogen coverage equal to $^1/_3$ ML is considered. In this case, the subsurface H atom can be located directly beneath CH_3 or at a subsurface site over

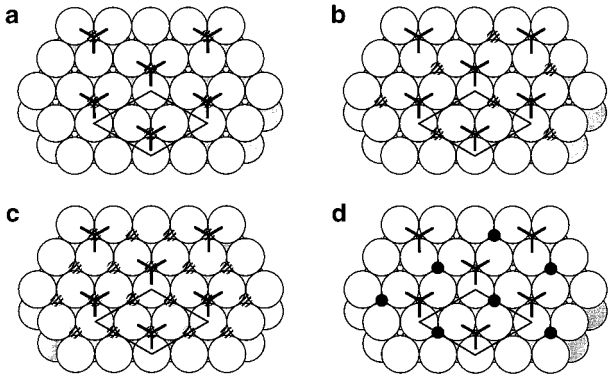

Figure 2. Schematic presentation of the predisposition for the coadsorption of CH_3 and H on the Ni(111) surface with CH_3 on a surface fcc hollow site and H on different sites: (a) subsurface octahedral site beneath CH_3 ($\theta_H = {}^1/_3$ ML); (b) neighbor subsurface octahedral site not directly below CH_3 ($\theta_H = {}^1/_3$ ML); (c) all the subsurface octahedral sites occupied ($\theta_H = 1$ ML); (d) surface fcc hollow site neighboring CH_3. CH_3 is represented by a 3 branch star indicating the C−H bonds while surface and subsurface H atoms are represented by full and hatched circles, respectively.

Table 2. Energies and Geometries for Coadsorption of H and CH_3 on Ni(111) $(\sqrt{3} \times \sqrt{3})R30°$ for the Configurations Shown in Figure 2

	a	b	c	d
E_{ad} (eV)	+0.60[a]	+0.45[a]	+0.49[b]	+0.21[a]
d_{C-Ni} (Å)[e]	2.15	2.12	2.15	2.19
z_C (Å)[f]	1.59	1.57	1.62	1.67
d_{H-Ni} (Å)[g]	1.83 (1.76)	1.75 (1.84)	1.85 (1.79)[c] 1.77 (1.89)[d]	1.63
z_H (Å)[f]	−1.13	−0.95	−1.19[c]; −1.01[d]	+0.75
Δd_{12} (%)[h]	+2.8	+2.8	+10.1	+1.1

[a] Coadsorption energy: $E_{ad} = E_{H-CH_3/Ni(111)} - E_{Ni(111)} - E_{CH_4}$. Here, the definition of this coadsorption energy is made in such a way that the final products, CH_4 + Ni(111), can be taken as the energy reference when discussing the reaction pathways. The positive value indicates the endothermicity of methane adsorption on the surface. [b] Coadsorption energy: $E_{ad} = E_{3H-CH_3/Ni(111)} - E_{2H/Ni(111)} - E_{CH_4}$; H atoms are located in octahedral subsurface sites. [c] H atom in the octahedral site just below the methyl group. [d] H atoms in the octahedral sites neighboring the methyl group. [e] d_{C-Ni}: bond length between C atom of the methyl group and the Ni atoms of the top layer. [f] z_C; z_H: height of the adsorbed species, CH_3 or H, with respect to the first nickel layer. [g] d_{H-Ni}: bond length between H atom and the Ni atoms of the top layer; in parentheses, bond length with the second Ni layer (for subsurface hydrogen only). [h] Δd_{12}: relative relaxation of the spacing between the two first nickel layers.

which there is no CH_3 (Figure 2a,b). The corresponding adsorption energies, as defined in Table 2, are respectively 0.60 eV (Figure 2a) and 0.45 eV (Figure 2b). The positive adsorption energy means that the coadsorption of H and CH_3 is less stable than methane. The experiment of Ceyer et al.[2] was carried out with a complete monolayer of H atoms on subsurface sites (Figure 2c). Under this condition, the coadsorption energy for H + CH_3, from our calculation, is 0.49 eV. The coadsorption energy for the configurations with the subsurface H atoms does not vary very strongly with the H coverage (see Table 2). When CH_3 and H are both adsorbed on the surface, the most stable coadsorption configuration is when they occupy the adjacent fcc sites (Figure 2d). At a coverage equal to $^1/_3$ ML, the adsorption energy is 0.21 eV. The geometries and the adsorption energies for the above coadsorption configurations are recapitulated in Table 2.

C. Reaction Pathways. The main purpose of the present work is to find energetically favorable reaction pathways and to

(33) Seetula, J. A.; Russell, J. J.; Gutman, D. *J. Am. Chem. Soc.* **1990**, *112*, 1347.

(34) Christmann, K.; Schober, O.; Ertl, G.; Neumann, M. *J. Chem. Phys.* **1974**, *60*, 4528.

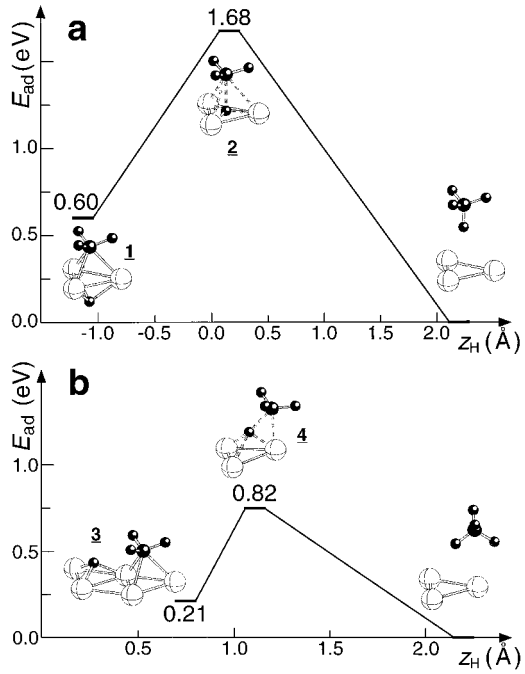

Figure 3. Structures of reactants, transition states, and products and the energetics (in eV) of reaction pathways: (a) one-step mechanism for the reaction of CH_3 with a subsurface H just below it; (b) reaction of CH_3 with a H adsorbed on a neighboring surface fcc hollow site. The chosen reaction coordinate z_H is the height of the H atom perpendicularly to the topmost Ni layer.

understand why the subsurface hydrogen is more active than the surface one for hydrogenating CH_3. For this, we examined a variety of reaction pathways through subsurface sites in parallel with the reaction pathway on the surface. On the basis of a simple symmetry argument, Ceyer and co-workers proposed a concerted reaction pathway.[2] They believe that the predisposition of CH_3 on the surface fcc site and the H atom beneath it on the subsurface octahedral site could lead straightforwardly to the formation of CH_4 with C_{3v} symmetry. Indeed, this appears to be an intuitively appealing reaction pathway. Therefore, we first examined this pathway and determined the corresponding transition state. As a surprise, it turned out that there is a quite high energy barrier (1.08 eV) along this 3-fold symmetric reaction pathway. A schematic presentation of the energy profile and of the transition state (TS) structure is given in Figure 3a. The geometry of this TS is described in more detail in Table 3. The energy barrier is much higher than that for the recombination of CH_3 with a H atom on the surface, i.e., 0.61 eV (see Figure 3b).[35] Hence, the selective hydrogenation of CH_3 by subsurface hydrogen observed experimentally cannot be accounted for by this concerted reaction pathway conjectured by Ceyer and co-workers.[2] This motivated us to look for other possible reaction pathways.

An alternative to the concerted pathway is a two-step pathway. The first step corresponds essentially to the emerging of the subsurface H atom, and the second step is the very formation of the C−H bond to yield CH_4. In the first step, the H atom makes its way out of the subsurface site while at the same time CH_3 opens the emerging path by sliding away. Such a sliding can be made in different directions, and two cases have been considered. In one case, the CH_3 slides toward a nearby top site and in the other case toward a hcp hollow site (see Figure 4). While the sliding of the CH_3 takes place simultaneously with the emerging of the subsurface H atom, the formation of the C−H bond starts only after the H atom has emerged. So, the reaction along this path proceeds with two distinct elementary steps. We have found the transition states of these two-step pathways for the two sliding directions described above. These paths are depicted in Figure 5, and the geometries are reported in Table 3. The nature of the different stationary points is specified in Table 3 by their order which gives the number of imaginary frequencies. The barrier for the emerging of the subsurface H does not depend sensitively on the direction in which CH_3 slides. In fact, there is a broad transition region for the subsurface H emerging. During its emerging, CH_3 can slide either toward the top site as shown in point **5** or to point **7** (Figure 5) or any intermediate point between them with only a very small energy change (less than 20 meV!). It is also interesting to note that the energy barrier for H emerging in the presence of a methyl group on the surface (0.25 eV) is not very different from that for H emerging to a clean surface (0.18 eV from our DFT calculation and 0.25 eV from the embedded-atom method).[36]

The second step, i.e., formation of the C−H bond, starts only after the subsurface H atom has come out on the surface. After crossing the first broad transition region locating between points **5** and **7** (Figure 5), the reacting system falls into a valley which contains the points **6** and **8** in Figure 5. These two structures are constraint minima which are also the transition states for CH_3 diffusing to a neighbor fcc hollow site. There exists a low-energy path connecting points **6** and **8**. At these points, the reacting system can have two possible fates: (1) the CH_3 sliding down (along the direction defined by the imaginary frequency found at **6** or **8**) into a near fcc hollow site without CH_4 formed; (2) crossing the second TS (Figure 5) and forming CH_4. The first process, i.e., CH_3 diffusing away into a neighbor fcc hollow site, proceeds downhill on the potential energy surface. Although the second process has an activation energy (0.42 eV) along the path described in Figure 5a (from **6** to **4**), it can take place without additional energy cost since the energy acquired in crossing the first barrier (0.47 eV) is enough to overcome the second one. So, the overall energy barrier to form CH_4 from the CH_3 and the subsurface H along the pathway described in Figure 5a is 0.27 eV (the first barrier in Figure 5a). Unlike the emerging of H, the energy barrier for the C−H bond formation depends on the direction in which CH_3 slides. The second barrier along the pathway described in Figure 5b is higher (note also that **9** corresponds to a high order stationary point). So, the C−H bond formation proceeds more favorably through **4**. The reaction of the CH_3 with a surface H proceeds exactly in the reverse way as for the fate 1 described above. Starting from the initial configuration depicted in Figure 3b (**3**), the CH_3 slides toward the top site and reaches the same geometry as **6** in Figure 5a, and further approach of the two reactants leads to the transition state, **4**, in Figure 3b (identical to the second TS in Figure 5a). This process is a monotonically uphill one on the potential energy surface and has a barrier equal to 0.61 eV.

(35) The recombination of CH_3 with a surface H atom is the reverse reaction of CH_4 dissociation. Theoretical studies for the dissociation of CH_4 on Ni(111) have been reported in the following: (a) Yang, H.; Whitten, J. L. *J. Chem. Phys.* **1992**, *96*, 5529 (with a cluster model for the Ni(111) surface). (b) Kratzer, P.; Hammer, B.; Nørskov, J. K. *J. Chem. Phys.* **1996**, *105*, 5595 (periodic supercell calculations similar to those performed in the present work). Taking into account of the different coverages, the energy at the TS we found (0.82 eV) is in qualitative agreement with the previous calculations: 0.73 eV in (a); 1.12 eV in (b). The experimental estimation is 0.53−0.55 eV (Lee, M. B.; Yang, Q. Y.; Ceyer, S. T. *J. Chem. Phys.* **1987**, *87*, 2724. Beebe, T. P.; Goodman, D. W.; Kay, B. D.; Yates, J. T. *J. Chem. Phys.* **1987**, *87*, 2305).

(36) Wonchoba, S. E; Truhlar, D. G. *Phys. Rev.* **1996**, *53*, 11222.

Table 3. Energies and Geometries of the Selected Configurations of $H-CH_3$ Corresponding to the Stationary Points along the Pathways of Figures 3 and 5

	E_{ad} (eV)[a]	z_H (Å)[c]	d_{C-H} (Å)[d]	d_{C-Ni} (Å)[b]	Δd_{12} (%)[e]	order[f]
1 (Figure 3a, 5)	+0.60	−1.13	2.72	2.15 (3)	+2.8	0
2 (Figure 3a)	+1.68	+0.15	1.83	2.49 (3)	+0.8	1
3 (Figure 3b)	+0.21	+0.75	2.66	2.19 (3)	+1.1	0
4 (Figure 3b, 5a)	+0.82	+1.16	1.52	2.07 (1)	−0.2	1
5 (Figure 5a)	+0.87	−0.18	2.78	1.95 (1)	+3.2	3
6 (Figure 5a)	+0.40	+0.76	2.28	1.98 (1)	+1.6	1
7 (Figure 5b)	+0.85	−0.06	2.41	2.04−2.31 (3)	+2.2	1
8 (Figure 5b)	+0.39	+0.77	2.57	1.99 (1)	+1.0	1
9 (Figure 5b)	+1.09	+0.93	1.54	2.40 (2)	+0.2	3

[a] Noninteracting CH_4 + clean Ni(111) as energy reference. [b] Distance between C and the Ni atom(s) of the top layer; the number of Ni nearest neighbors is given in parentheses. [c] z_H: height of the H atom with respect to the first nickel layer. [d] d_{C-H}: bond length between the reactive H atom and the C atom. [e] Δd_{12}: relative relaxation of the spacing between the two first nickel layers. [f] Order: number of imaginary frequencies of the stationary point.

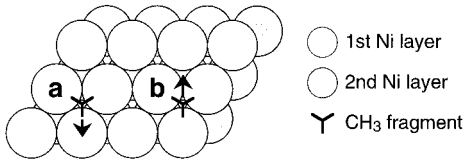

Figure 4. Sketch of two possible sliding directions of CH_3 in a two-step mechanism for its reaction with a subsurface H atom: (a) sliding toward a top site; (b) sliding toward a hcp hollow site.

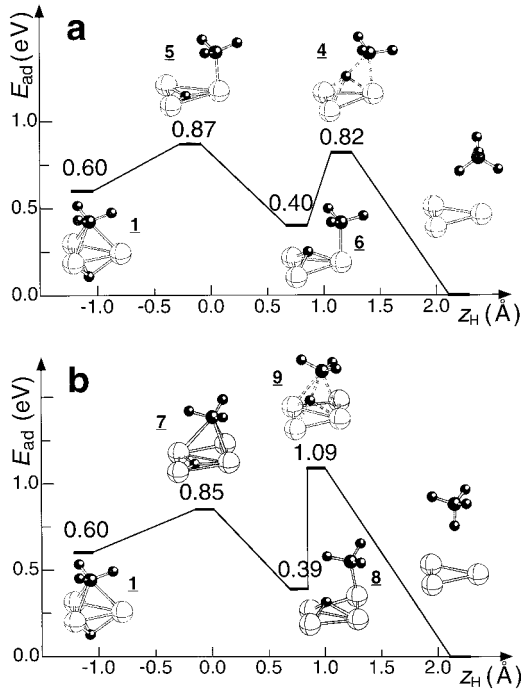

Figure 5. Structures of reactants, transition states, and products and the energetics of the two-step reaction pathways: (a) CH_3 sliding toward a top site; (b) CH_3 sliding toward a hcp hollow site.

Now, from these results we can obtain a quite satisfactory interpretation of the fact that CH_3 is selectively hydrogenated by the subsurface H atoms but not by their counterparts on the surface. First, the energy barrier for the emerging of the subsurface hydrogen (0.25−0.27 eV) is much lower than that for the reaction of CH_3 with a H atom on a surface site (0.61 eV). Second, the barrier for the emerging of the subsurface H atoms plays the role of an energy filter. If the tunneling effect is disregarded, only H atoms acquiring an energy exceeding that of the transition state can come out on the surface. These H atoms just coming out from subsurface sites are much more energetic than the surface adsorbates already thermalized with the substrate and can readily react with the nearby CH_3. This accounts satisfactorily for the experimental finding[2] that the methane formation is observed at the same temperature as that for the emerging of the subsurface hydrogen. The transition state for this H emerging step is found precisely at the geometry with the H atom in the plane of the surface Ni atoms. At this transition state, the relaxation of the surface Ni atoms has an important effect on the energy barrier (a frozen Ni surface leads to a barrier of 1.05 eV). We also examined a variety of possible emerging processes of the subsurface H atoms. The most favorable path is through a site not capped by CH_3 (Figure 2b). This can lead to a configuration corresponding to the initial one for the CH_3 with a surface H atom (see the initial configuration in Figure 3b). After this emerging, the reaction path becomes identical to that for the recombination on the surface. Since the surface recombination is inefficient for the hydrogenation of CH_3, the H atoms emerging through the uncovered sites stay adsorbed on the surface. The remaining subsurface H atoms can emerge either through a site capped by a CH_3 or by a surface H. We found that the subsurface H emerges more easily through a site capped by CH_3 than through one capped by H. The former emerging process leads readily to the formation of methane.

After finding the most favorable reaction pathway, i.e., the two-step one (first the emerging of H and then formation of C−H bond), we have also made some analysis to understand why the symmetric concerted path is unfavorable. From the geometry of the TS on the concerted reaction pathway (Figure 3a), one can see that at this point CH_3 is pushed quite far away from the substrate. One intuitively appealing explanation for the high energy at this point is that the CH_3 loses too much interaction with the substrate before the C−H bond is formed. To corroborate this, we have carried out the following calculation: bringing CH_3 to this point but keeping the H atom on the octahedral subsurface site. This calculation provides us a measure for the energy increase due to the interaction loss of the CH_3 with the substrate which is 0.35 eV. This moderate increase cannot account for the high energy barrier along the concerted pathway. In fact, the high barrier results from quite a strong repulsion between H and CH_3. At this TS, there exists still quite a good interaction between CH_3 and the substrate. Hence, the sp^3 orbital of CH_3 is still quite saturated by its interaction with the three Ni atoms beneath it. Thus, we can deduce that the Pauli repulsion arises between H and CH_3. So, the high energy barrier along the concerted reaction pathway is essentially due to a strong Pauli repulsion between H and CH_3. This interpretation can account as well for the height of the second barriers for the reaction pathways presented in Figure 5. Along the pathway presented in Figure 5b, the sp^3 orbital of the CH_3 interacts with two Ni atoms of the substrate at the

second TS and is more saturated than in the case of CH_3 sliding toward the top site where the sp^3 orbital interacts only with one Ni atom (Figure 5a). Thus, the Pauli repulsion is stronger in the former case and this is why the corresponding energy barrier is higher.

IV. Conclusions

The results reported here supply a theoretical support to the new mechanism of heterogeneous catalysis through subsurface sites discovered by Ceyer and co-workers.[2] Moreover, we find that the microscopic reaction pathway for the hydrogenation of CH_3 on Ni(111) by subsurface hydrogen is a two-step one instead of the concerted one believed by Ceyer et al. The emerging of the subsurface hydrogen is a moderately activated process. Nevertheless, the energy barrier of this process plays the role of a filter which yields more active species than the surface adsorbates which are in thermal equilibrium with the substrate. The higher reactivity of the subsurface species originates from the higher potential energy of the metastable state in which they are placed. Subsurface species can be created in an UHV experiment (ultrahigh vacuum) only by using molecular beams with sufficient energy. Alternatively, they could be also formed readily in a more realistic high-pressure catalytic environment. Once the energy barrier is crossed by the H atoms emerging from a subsurface site, the acquired extra potential energy makes them behave like "hot" reactants. Putting one reactive species into a metastable state, e.g., by hammering it into a subsurface site, is a nice way to store potential energy whose subsequent release can increase the reactivity of the reactant. We believe that this is a widely useful means to produce more active species in heterogeneous catalysis. Our finding here accounts satisfactorily for a new and general class of catalytic reactions. It highlights the usefulness of metastable subsurface species. While hammering with a molecular beam is a laboratory means to produce such subsurface species, increasing the pressure in a reactor could be a more practical way to obtain subsurface reactants in industrial applications. This implies also that the reactivity observed under high-pressure conditions used in many applications can be very different from that obtained under UHV conditions widely used in surface science investigations.

Acknowledgment. We thank John K. Brennan for reading carefully the manuscript. This work has been undertaken within the GdR, Dynamique Moléculaire Quantique Appliquée à la Catalyse, a joint project of the CNRS, Universität Wien, Institut Français du Pétrol, and Total. Computer time on the Cray T3E has been allocated for the present work by IDRIS of the CNRS (project 990609).

JA983975G